Jurnal Teknologi

Full Paper

SIMULATION STUDY ON THE ELECTRICAL PERFORMANCE OF EQUILIBRIUM THIN-BODY DOUBLE-GATE NANO-MOSFET

Ooi Chek Yee[a*], Lim Soo King[b]

[a]Faculty of Information and Communication Technology, Universiti Tunku Abdul Rahman, Jalan Universiti, Bandar Barat, 31900 Kampar, Perak, Malaysia
[b]Lee Kong Chian Faculty of Engineering and Science, Universiti Tunku Abdul Rahman, Jalan Sungai Long, Bandar Sungai Long, Cheras, 43000 Kajang, Selangor DarulEhsan, Malaysia

Article history
Received
5 January 2015
Received in revised form
18 March 2015
Accepted
1 August 2015

*Corresponding author
ooicy@utar.edu.my

Graphical abstract

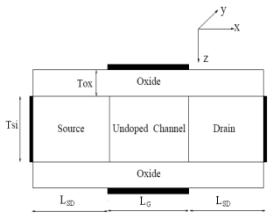

Abstract

This paper presents a numerical simulation study for electrical characteristics of double-gate (DG) nano-MOSFET at equilibrium thin-body condition. The electrical characteristics which are studied include subband energy (including unprimed and primed subbands), 2D electron density at 77K and 300K ambient temperatures, transmission coefficient, average electron velocity and ballistic current. The ranges of silicon body thickness T_{Si} are 1.0 nm, 1.5 nm and 2.0 nm. The electron transport models used in simulation tool covered quantum model and classical model. Simulation output data are also compared with theoretical discussion.

Keywords: Ballistic, classical, nanometer, temperature effects, wave nature, particle

Abstrak

Kajian ini menjalankan simulasi sifat-sifat elektrik nano-MOSFET pada keadaan seimbang. Sifat-sifat ini termasuk jalur tenaga (jalur unprimed dan primed), ketumpatan elektron 2D pada suhu 77 K dan 300 K, pemalar pengaliran, kelajuan purata elektron dan arus ballistik. Linkungan ketebalan lapisan silikon adalah 1.0 nm, 1.5 nm dan 2.0 nm. Model pengangkutan elektron yang digunakan dalam perisian simulasi termasuk model kuantum dan model klasikal. Data hasil simulasi dibandingkan dan dianalisikan dengan teori.

Kata kunci: Ballistik, klasik, nanometer, kesan suhu, sifat gelombang, zarah

1.0 INTRODUCTION

DG nano-MOSFET with silicon channel length at 10 nm is studied in this paper, and this truly nanometric transistor is approaching the ballistic transport regime since the phonon mean free path scattering for electron in silicon is 76Å (7.6 nm). When the channel of this nano-MOSFET is thin enough (less than 5 nm, typically), the energy levels splitting will be significantly larger than thermal voltage (0.025 eV at 300 K), and electrons are only able to occupy the bottom subbands without hopping to higher levels. In this case, Schrödinger equation can be used to solve for wavefunction which in turn is used to obtain electron spatial distribution [1-4]. In the Possion solver used in the simulation tool, the electron density, n is given by

$$n = N_C \mathcal{F}_{1/2}\left(\frac{E_F - E_C}{k_B T}\right) \quad \text{Equation (1)}$$

In non-degenerate limit, the Fermi-Dirac integral can be simplified to become

$$n = N_C \exp\left(\frac{E_F - E_C}{k_B T}\right) \quad \text{Equation (2)}$$

where E_F = energy of the Fermi level
E_C= energy of conduction band
k_B= Boltzmann constant
T= Temperature
N_C = effective density of states in the conduction band

In this simulation project, the material is silicon and wafer orientation is (001)/channel transport direction is [100]. The conduction band in silicon consists of two set of subbands, that is unprimed subbands and primed subbands. The output results of this simulation project contain data regarding 1st and 2nd unprimed subbands as well as 1st primed subband. Because of the heavier electron effective mass, unprimed subbands have relatively lower bound state energies as compared to the lighter electron effective mass of primed subband. Therefore, electrons basically occupied these three lower energy subbands [5-9].

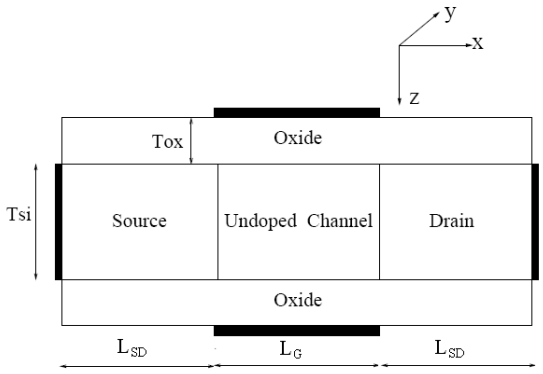

Figure 1 2D structural design of DG nano-MOSFET

Consider the electron movement in a 2D dimension region of the channel, L_Z (channel thickness) x L_X (device length), the 2D Schrödinger equation is given by

$$\left(-\frac{\hbar^2}{2m^*}\left(\frac{\partial^2}{\partial x^2}+\frac{\partial^2}{\partial z^2}\right) - E\right)\psi(x,z) = 0 \quad \text{Equation (3)}$$

where $\hbar$ = reduced Planck's constant
m^* = electron effective mass (unprimed and primed subband)
E= electron energy
$\psi(x,z)$ = wavefunction

Assume a product solution of the form

$$\psi(x,z) = \psi_x(x)\psi_z(z) \quad \text{Equation (4)}$$

Equation (3) becomes

$$\left(\frac{1}{\psi_x}\frac{\partial^2}{\partial x^2}\psi_x + \frac{1}{\psi_z}\frac{\partial^2}{\partial z^2}\psi_z + \frac{2m^*}{\hbar^2}E\right) = 0 \quad \text{Equation (5)}$$

The time-dependent wavefunction for an electron is

$$\Psi(\mathbf{r},t) = \psi(\mathbf{r})e^{-\frac{iEt}{\hbar}} = A_0 e^{i\mathbf{k}\cdot\mathbf{r}} e^{-\frac{iEt}{\hbar}} \quad \text{Equation (6)}$$

where **r** = position vector = $a_x x + a_z z$ (in rectangular coordinates; a is unit vector)
k = wavevector = $a_x k_x + a_z k_z$

The time-independent wavefunction is obtained by putting t=0,

$$\Psi(\mathbf{r},0) = \psi(\mathbf{r}) \quad \text{Equation (7)}$$

The allowed discrete values of energy are given by

$$E_{n_x,n_z} = \frac{\hbar^2\pi^2}{2m^*}\left(\left(\frac{n_x}{L_x}\right)^2 + \left(\frac{n_z}{L_z}\right)^2\right) \quad \text{Equation (8)}$$

where n_x and n_z = quantum numbers.

Degenerate is the situation where states with different quantum numbers but have the same energy as will be analyzed in next section [10]. For much of the simulation results of this project, consider only the single particle Schrödinger equation. This assumption seems not suitable since the number of electrons is very large in typical silicon channel. However, the single particle Schrödinger equation usually can be applied due to the fact that for silicon, assumption that electrons are non-interacting to each other is almost valid because of screening effect which is related to the Pauli exclusion principle. Electrons repel each other because (i) like charges repel each other and, (ii) electrons with the same spin will avoid each other. Since no two electrons can have the same state, the probability of electrons with the same spin not located near each other is high. Therefore, in silicon electrons movements are independent of each other.

2.0 RESULTS, ANALYSIS AND DISCUSSION

In this simulation project, all biasing voltages are set to zero volts. Figure 2 shows the 1st unprimed subband energy along the channel at equilibrium condition for various silicon channel thickness T_{Si} at 300K with ballistic transport using Green's function approach [11-15].

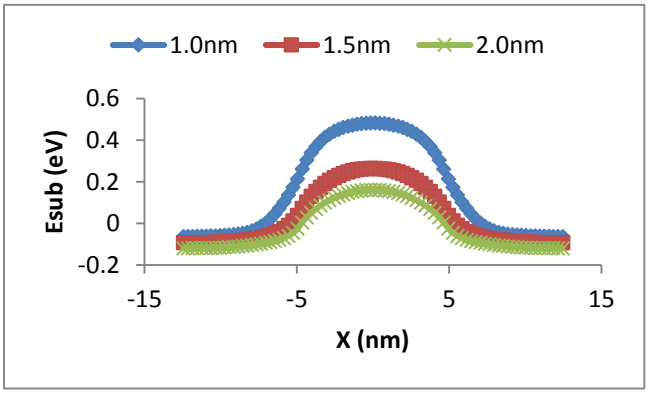

Figure 2 1st unprimed subband energy along the channel at equilibrium condition for various silicon channel thickness T_{Si} at 300K with ballistic transport using Green's function approach

Table 1 Silicon channel thickness and corresponding 1st unprimed subband energy

Thickness (nm)	1st unprimed subband energy at middle of the channel (eV)
1.0	0.50
1.5	0.27
2.0	0.16

From Figure 2 and Table 1, as T_{Si} decreases, potential barrier height increases. This situation causes more backscattering electrons and so lesser electrons will flow to the channel for thinner T_{Si}. Therefore, 2D electron density distribution in the channel will also be smaller for thinner T_{Si}. Also, steeper slope can be observed in the semilog plot of 2D electron density for thinner T_{Si}. Figure 3 exhibits this phenomenon.

From Equation (2), at fixed temperature 300K, N_C is fixed, so

$$n \propto \exp\left(\frac{E_F - E_C}{k_B T}\right) \qquad \text{Equation (9)}$$

At source and drain contacts, when T_{Si} increases, 2D electron density n in source and drain contact increases (see Figure 4). When n increases, from Equation (9), conduction band energy E_C should reduces since energy of the Fermi level is fixed. So, thicker source/drain contacts have smaller energy level value as shown in Figure 2. With thinner T_{Si}, from Figure 4, 2D electron density at source/drain contacts reduces. From Equation (9), E_C should be higher.

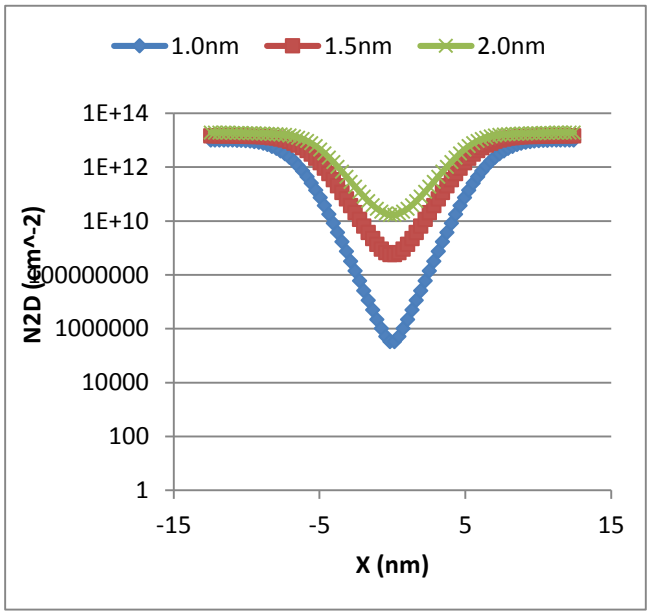

Figure 3 Semilog plot of 2D electron density along the channel for various silicon channel thicknesses at 300 K

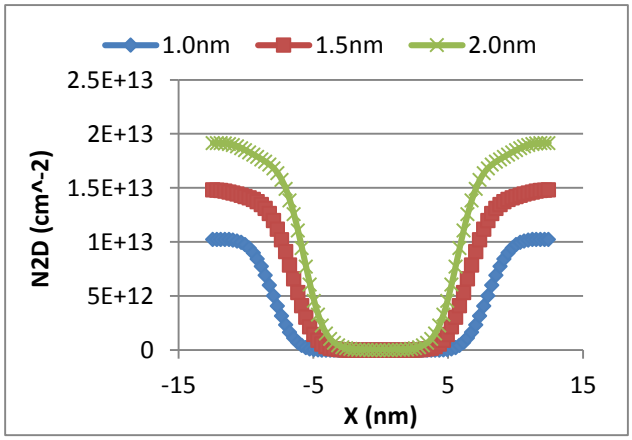

Figure 4 Normal plot of 2D electron density along the channel for various silicon channel thicknesses at 300 K

From Figure 2 and Figure 3, in the channel region, T_{Si}=2.0 nm has the lowest 1st unprimed subband energy and so this subband is the most populated with electrons. Thus, its 2D electron density is the highest among all the thicknesses studied.

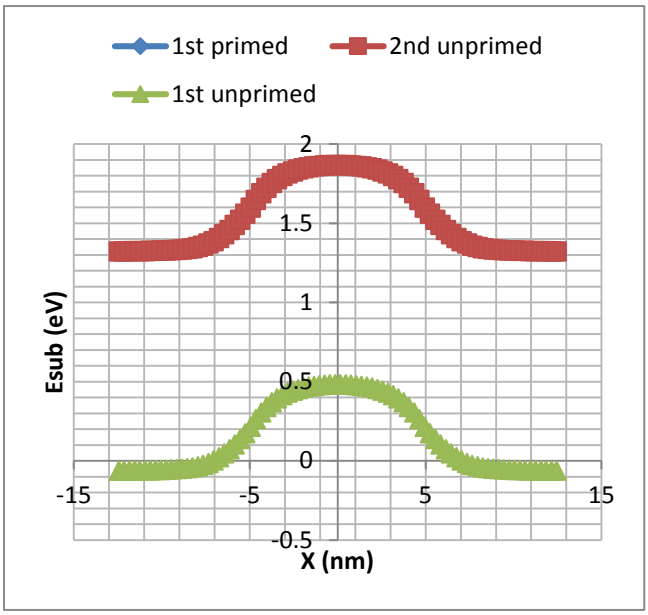

Figure 5 Energy subbands profile along the channel for channel thickness 1.0 nm

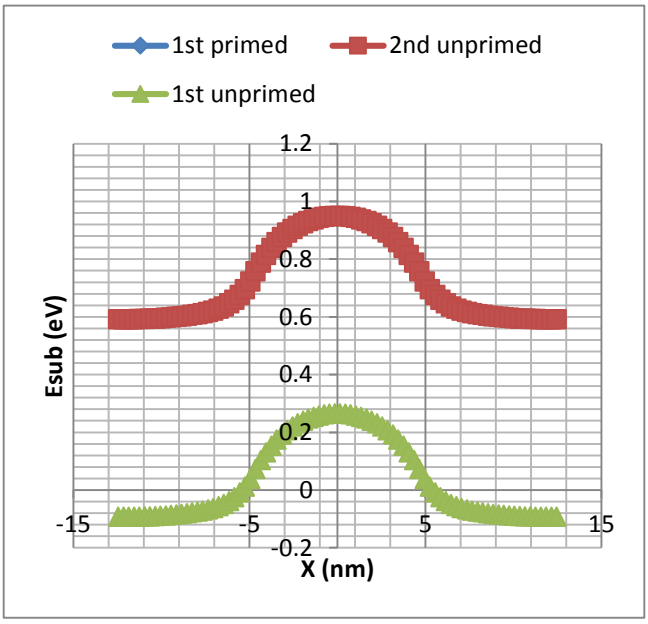

Figure 6 Energy subbands profile along the channel for channel thickness 1.5 nm

Figure 5, Figure 6 and Figure 7 show the subbands energy profile for different T_{Si} with Green's function approach at 300K. Each figure has 1st and 2nd unprimed subbands as well as 1st primed subband. The 2nd unprimed has same energy as the 1st primed subband. Both of these two subbands have different quantum numbers. This phenomenon is called degenerate. As energy increases, density of states (DOS) decreases but when a new subband is reached, DOS increases suddenly and then gradually decreases again. There are several ways to reduce channel DOS, (i) reducing the number of populated subband by enhancing confinement. In other words, uses thinner channel which is the topic studied in this project. Other ways include (ii) introducing mechanical strain and using different wafer orientation, and (iii) just using low DOS alternative materials for channel, for instance GaAs has lower DOS than silicon (001)/[100] material which is used in DG nano-MOSFET of this project.

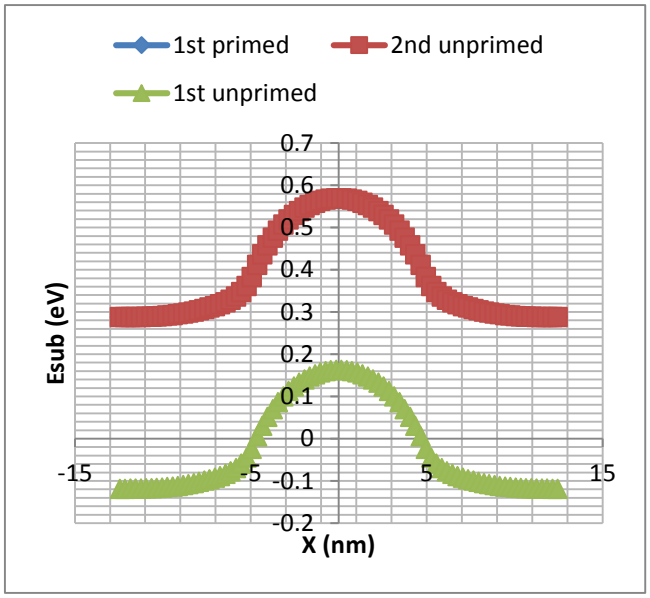

Figure 7 Energy subbands profile along the channel for channel thickness 2.0 nm

Table 2 Silicon channel thickness and corresponding energy levels separation

Thickness (nm)	Separation between energy levels (eV)
1.0	1.30
1.5	0.60
2.0	0.40

Table 3 Simulated and calculated value of energy levels

Energy levels	simulated energy (eV)	calculated energy (eV)
1st unprimed subbans	0.25	0.261
2nd unprimed subband	0.95	0.959
1st primed subband	0.95	0.899

Table 2 is the result collected from Figure 5, Figure 6 and Figure 7. From Table 2, as T_{Si} decreases, separation energy gap between subbands

increases. From Figure 3 and Figure 4, in the channel region the charge density is relatively low compared to source and drain regions. Therefore, the 1st unprimed subband accounts for almost all of the channel charges. However, since the source and drain contacts are N^+ heavily doped with donor, the higher subbands also contribute to the total 2D charge, thereby making a single subband treatment inadequate. Therefore, two more nearest subbands are considered in this simulation project. Now, let compare the quantum energy levels between simulated data and theoretical calculation from Equation (8). Let consider the case for channel thickness 1.5 nm and Table 3 is obtained. In Table 3 theoretical calculation using Equation (8), channel thickness is 1.5 nm and channel length is 10 nm. The electron effective mass for 1st and 2nd unprimed subbands is taken to be 0.98xfree electron mass where as the 1st primed subband electron effective mass is lighter, which is taken to be 0.19xfree electron mass.

The chemical potential effects are included in the calculation for unprimed subbands. In this case, the theoretical formulae for the unprimed spacing between the two unprimed quantum energy levels for T_{Si}=1.5 nm is given by

$$E_n - E_{n-1} = 0.261(2n-1)\ \text{eV} \qquad \text{Equation (10)}$$

For unprimed subband in this case

$$E_2 - E_1 = 0.261(3)\ \text{eV} = 0.783\ \text{eV}$$

From simulation results in Table 3, it is equal to 0.700eV. The Fermi level is defined as the value of chemical potential at T=0K. Chemical potential is basically could be think as approximately the energy needed to add Nth electron to a system of N-1 electrons. So, in this simulation project, it can be related in 1st and 2nd unprimed subbands.

Figure 5, Figure 6 and Figure 7 show that 2nd unprimed energy level is the same as 1st primed energy level. This case is called degenerate since both of them have same energy but different quantum levels. This degeneracy causes the graph of energy versus transmission coefficient (Figure 8) to be almost continuous flat between total transmission coefficient 1 and total transmission coefficient 3. In ballistic nano-MOSFET using Green's function, the current flow is controlled by transmission coefficient which is the probability of electrons to be able to transmit through the channel in a single subband. In this simulation project, 2 unprimed subbands and 1 primed subband are simulated, thus total transmission coefficient is simply addition of transmission coefficients for all these 3 subbands. So, in this project, the maximum obtainable transmission coefficient is thus 3. Thinner T_{Si} causes higher potential barrier which resulted in larger energy level shift for thinner T_{Si} in Figure 8.

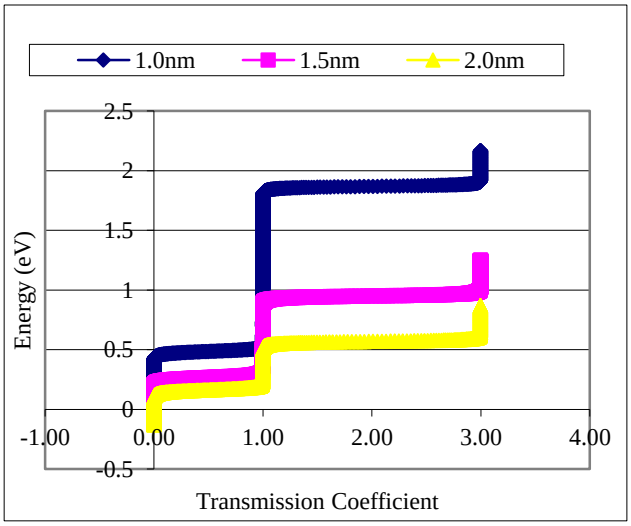

Figure 8 Transmission coefficients curve for various channel thicknesses simulated at 300K

Total transmission coefficient value from 0 to 1 is caused by 1st unprimed subband. Meanwhile, total transmission coefficient value from 1 to 3 is caused by 2nd unprimed subband and 1st primed subband which formed degeneracy.

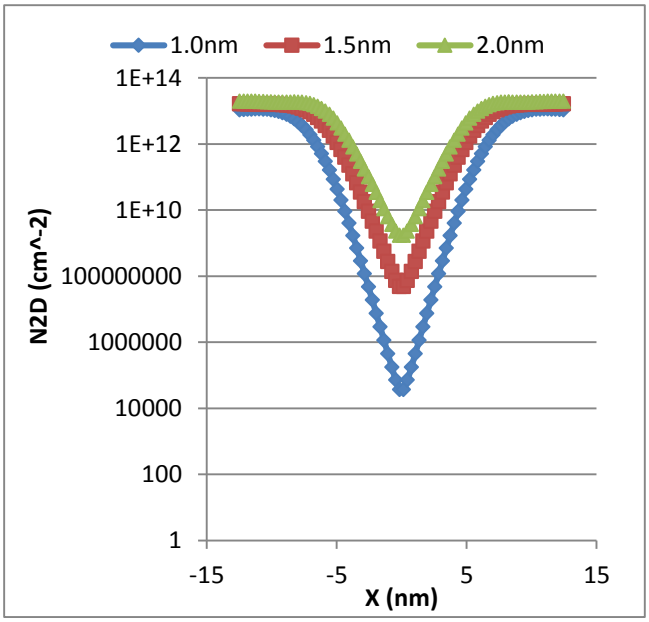

Figure 9 Semilog plot of 2D electron density along the channel for various silicon channel thicknesses at 77K.

Now, comparing Figure 3 and Figure 9 where both of these two figures are 2D electron density along the

channel using quantum model semilog plot for 300K and 77K, respectively. These two plots could be analyzed with the following expression

$$n_{(qm)} = n_{(conv)} \exp\left\{\frac{E_{g(qm)} - E_{g(conv)}}{2k_B T}\right\} \quad \text{Equation (11)}$$

where $n_{(qm)}$= electron concentration after quantum mechanical correction
$n_{(conv)}$ = conventional electron concentration
$E_{g(qm)}$ = quantum level energy
$E_{g(conv)}$ = energy gap for conventional model

Taking the 1st unprimed subband for T_{Si} = 1.0 nm for elaboration. The 1st unprimed subband for 300K and 77K are very close to each other so that their difference could be ignored. From Figure 2, this value $E_{g(qm)}$ = 0.5eV. Referring to Equation (11), the exponential term value for 300K is larger than that of 77K. So, the electron density in the channel is higher for 300K case. The channel region has less electron density than source/drain regions because the probability of electron to overcome the subband is become lesser and lesser. Energy of electrons in equilibrium condition without voltage biasing comes from thermionic emission.

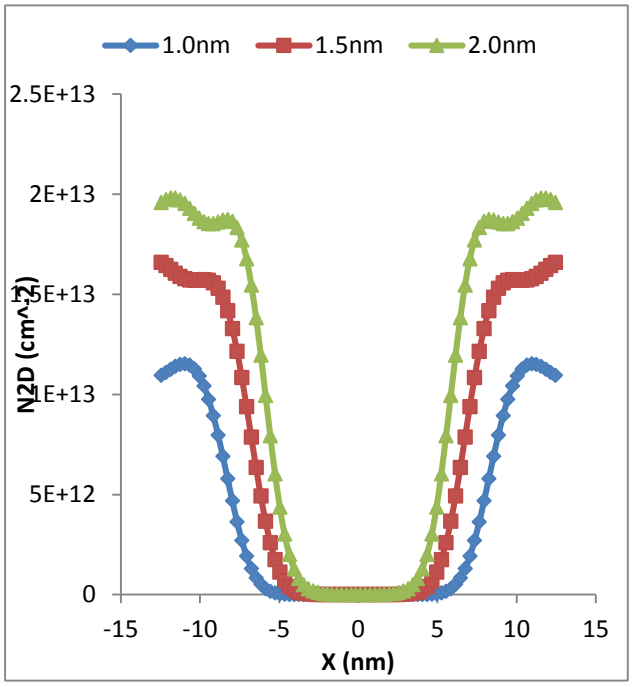

Figure 10 Normal plot of 2D electron density along the channel for various silicon channel thicknesses at 77K using quantum model

Figure 10 shows the 2D electron density distribution for various T_{Si} at 77 K using quantum model. Figure 10 shows some oscillations near source and drain regions whereas Figure 4 which is the same plot with same design parameters but simulated at 300 K doesn't exhibit such oscillations. In Figure 10, T_{Si} = 1.0 nm curve indicates less wave oscillation nature (longer wavelength) in source/drain regions compared with T_{Si} = 2.0 nm curve. This may due to quantum confinement effect where T_{Si} = 2.0 nm has transition between bands because the energy bands are close to each other.

For an electron of mass m in an equilibrium condition, the Schrödinger equation is

$$i\hbar \frac{\partial \Psi_{(r,t)}}{\partial t} = \left(-\frac{\hbar^2}{2m}\nabla^2\right)\Psi_{(r,t)} \quad \text{Equation (12)}$$

Assuming a product form for the wavefunction

$$\Psi(\mathbf{r},t) = \psi(\mathbf{r})g(t)$$

where $g(t) = e^{-iEt/\hbar}$

Substituting the wavefunction product into Equation (12) results in

$$\left(-\frac{\hbar^2}{2m}\frac{1}{\psi(r)}\nabla^2\psi(\mathbf{r})\right) = i\hbar\frac{1}{g(t)}\frac{\partial g(t)}{\partial t} \quad \text{Equation (13)}$$

Equation (13) can be used to explain the effects of temperature on oscillations in electron density distribution seen in above figures. The left hand side of Equation (13) is function of position (spatial) but not time, while the right hand side is a function of time but not position. This situation arises only when each side is equal to the same constant called E (energy). So,

$$\left(-\frac{\hbar^2}{2m}\nabla^2\psi(\mathbf{r})\right) = E\psi(\mathbf{r}) \quad \text{Equation (14)}$$

$$i\hbar\frac{\partial g(t)}{\partial t} = Eg(t) \quad \text{Equation (15)}$$

There are two operators for quantum mechanics; firstly is the momentum operator which is related to spatial part of a plane-wave function by

$$\psi(\mathbf{r}) = Ae^{\mathbf{ikr}}$$

and after applying the operator

$$\hat{o} = -i\hbar\frac{\partial}{\partial \mathbf{r}} \quad \text{Equation (16)}$$

to function $\psi(\mathbf{r})$ leads to

$$-i\hbar\frac{\partial}{\partial \mathbf{r}}\psi(\mathbf{r}) = -i\hbar\frac{\partial}{\partial \mathbf{r}}Ae^{\mathbf{ikr}} = \hbar\mathbf{k}\psi(\mathbf{r}) = \mathbf{p}\psi(\mathbf{r}) \quad \text{Equation (17)}$$

where $\mathbf{p} = \hbar\mathbf{k}$ is the momentum. Hence Equation (16) is called the momentum operator, expressed as

$$\hat{\mathbf{p}} = -i\hbar\frac{\partial}{\partial \mathbf{r}}$$

In Figure 4 and Figure 10, as temperature increases, energy of electron increases, so does the velocity of electron. This causes the momentum of the electron increases. Hence, electron behaves more like particle in higher temperature 300K and thus oscillation patterns are not observed at high temperature.

Secondly, there is energy operator which is

$$\hat{\mathrm{E}} = \mathrm{i}\hbar\frac{\partial}{\partial \mathrm{t}} \qquad \text{Equation (18)}$$

Consider the temporal dependence of g(t)

$$\mathrm{g(t)} = \mathrm{e}^{-\mathrm{iEt}/\hbar}$$

obtaining

$$\hat{\mathrm{E}}\mathrm{g(t)} = \mathrm{i}\hbar\frac{\partial}{\partial \mathrm{t}}\mathrm{g(t)} = \mathrm{i}\hbar\frac{\partial}{\partial \mathrm{t}}\mathrm{e}^{-\mathrm{iEt}/\hbar} = \hbar\frac{\mathrm{E}}{\hbar}\mathrm{g(t)} = \mathrm{Eg(t)}$$

Equation (19)

In Figure 4 and Figure 10, as temperature reduces, energy of electron reduces. So, the effects of temporal dependence of energy in g(t) increases. Thus, electron behaves more like wave plane in low temperature 77K and thereby oscillation patterns are observed in low temperature. This is the case of electron has a particle-wave duality property.

Put in other words, quantum charge density exhibits oscillations caused by interference of incident and reflected electron waves near source/drain regions at low temperature 77K. However, at high temperature when Poisson equation is used to solve for potential, the charge oscillations disappear, resulting in smooth profile. In semiclassical model (see Figure 11) no such oscillations are observed even at low temperature 77K since semiclassical model considered particle nature of electron through Boltzmann Transport Equation (BTE).

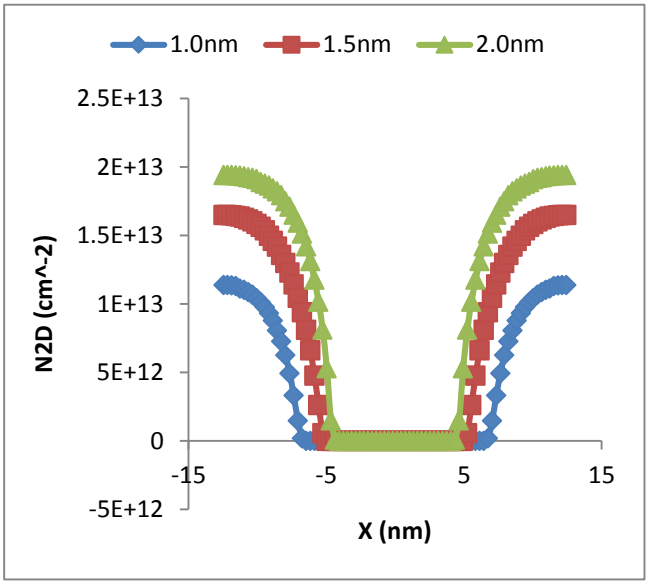

Figure 11 Normal plot of 2D electron density along the channel for various silicon channel thicknesses at 77K using semiclassical model

Now, let focuses on the result of average electron velocity and current flow in equilibrium condition (without voltage biasing at all terminals). Average electron velocity in source/drain (heavily N+ doped) and channel (intrinsic) should all be zero because no drift electric field due to no biasing voltages [16, 17]. This is shown by Figure 12 below. In source/drain contacts which are heavily N+ doped, maximum individual electron velocity value should be lower than channel maximum individual electron velocity due to impurities scattering in source/drain contacts. Since average electron velocity is zero as shown in Figure 12, the current flow should also be zero. This current flow phenomenon can be analyzed by using Natori-Lundstrom models of ballistic transport.

Firstly, let explained the zero current flow by using Natori model of ballistic transport. Two important assumptions are considered: (i) nano-MOSFET source and drain are assumed to be electron reservoirs in equilibrium condition, (ii) negligible short channel effects are assumed. In this project, 1st and 2nd unprimed as well as 1st primed subbands are simulated. So, the electron flux $\mathrm{F_s^+}$ emitted from the source in equilibrium and entering the channel can be expressed as

$$\mathrm{F_s^+} = \frac{(2\mathrm{kT})^{3/2}}{\pi^2\hbar^2}\left[\left\{\sqrt{\mathrm{m_{cL}}}\mathcal{F}_{1/2}\left(\frac{\mathrm{E_{Fs}} - \mathrm{E_1^L}}{\mathrm{kT}}\right) + \sqrt{\mathrm{m_{cL}}}\mathcal{F}_{1/2}\left(\frac{\mathrm{E_{Fs}} - \mathrm{E_2^L}}{\mathrm{kT}}\right)\right\} + \sqrt{\mathrm{m_{cT}}}\mathcal{F}_{1/2}\left(\frac{\mathrm{E_{Fs}} - \mathrm{E_1^T}}{\mathrm{kT}}\right)\right]$$

Equation (20)

where $m_{cL} = m_t$ =unprimed subband conductivity electron effective mass
$m_{cT} = \left(m_l^{1/2} + m_t^{1/2}\right)^2$ = primed subband conductivity electron effective mass
m_t= transverse electron effective mass
m_l=longitudinal electron effective mass
$E_{1,2}^L$=1st and 2nd unprimed subband energies
E_1^T=1 primed subband energy
$\mathcal{F}_{1/2}$=Fermi integral of order ½

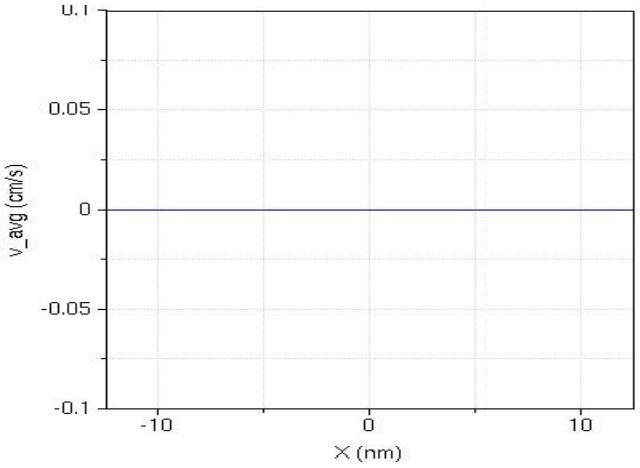

Figure 12 Average electron velocity along the channel at equilibrium conditio

Electron flux F_d^- emitted from the drain to the source has a similar expression with F_s^+ except $E_{Fd} = E_{Fs} - qV_{ds}$. Since V_{ds}=0V and V_{gs}=0V, $E_{Fd} = E_{Fs}$=energy level of the Fermi level of source and drain.

$$F_d^- = \frac{(2kT)^{3/2}}{\pi^2\hbar^2}\left[\left\{\sqrt{m_{cL}}\mathcal{F}_{1/2}\left(\frac{E_{Fd} - E_1^L}{kT}\right) + \sqrt{m_{cL}}\mathcal{F}_{1/2}\left(\frac{E_{Fd} - E_2^L}{kT}\right)\right\} + \sqrt{m_{cT}}\mathcal{F}_{1/2}\left(\frac{E_{Fd} - E_1^T}{kT}\right)\right] \quad \text{Equation (21)}$$

At V_{ds}=0V, $E_{Fd} = E_{Fs}$ coincides with inversion layer Fermi level. The ballistic current flowing from source to drain is

$$I_d^{BAL} = qT(E)(F_s^+ - F_d^-) = 0 \quad \text{Equation (22)}$$

since $F_s^+ = F_d^-$. T(E) is the transmission coefficient.

Secondly, let compares the above result with Lundstrom model which includes the backscattering coefficient r, which is defined as the ratio between electron flux backscattered to the source by scattering divided by the electron flux emitted by the source. When no biasing voltage is applied to nano-MOSFET terminals, the backscattering coefficients have the same value at the source and drain side. The current flow is given by

$$I_d^{QBAL} = qT(E)[F_s^+ - rF_s^+ - (1 - r)F_d^-] \quad \text{Equation (23)}$$

Since $F_s^+ = F_d^-$,

$$I_d^{QBAL} = qT(E)[F_s^+ - rF_s^+ - F_d^- + rF_d^-] = 0 \quad \text{Equation (24)}$$

Therefore, Natori model and Lundstrom model of ballistic transport have the same current flow result at equilibrium condition (no voltage biasing) [18].

3.0 CONCLUSION

When the channel thickness of nano-MOSFET is thin enough (usually less than 5 nm), the splitting of energy levels are large enough. In room temperature 300K, the splitting of energy levels is larger than thermal voltage. Therefore, only the lowest few energy bands are populated and this situation is able to explain the electrical characteristics of nano-MOSFET well. In equilibrium state (no voltage biasing at terminals), the electronic charge distribution is symmetry causing zero net current flow even though the electron individual velocity is not zero. However, the average electron velocity is zero at this equilibrium condition. In non-equilibrium state, charge distribution is not symmetry anymore and net current flows due to Fermi levels difference between source and drain.

References

[1] Zhibin Ren. 2001. *Nanoscale MOSFETs: Physics, Simulation and Design.* Purdue University.
[2] Xufeng Wang. 2010. *NanoMOS 4.0: A Tool to Explore Ultimate Si Transistors and Beyond.* Purdue University.
[3] Prashant Subhash Damle. 2003. *Nanoscale Device Modeling: From MOSFETs to Molecules.* Purdue University.
[4] Ramesh Venugopal. 2003. *Modeling Quantum Transport in Nanoscale Transistors.* Purdue University.
[5] Xufeng Wang. *NanoMOS 3.5 First Time User Guide.* Network for Computational Nanotechnology (NCN). Purdue University.
[6] Zhibin Ren, Ramesh Venugopal, Sebastien Goasguen, Supriyo Datta, Mark S. Lundstrom. 2003. NanoMOS 2.5: A Two-Dimensional Simulator for Quantum Transport in Double-gate MOSFETs. *IEEE Transactions on Electron Devices.* 50(9): 1914-1925.
[7] Victor A. Sverdlov, Thomas J. Walls, Konstantin K. Likharev. 2003. Nanoscale Silicon MOSFETs: A Theoretical Study. *IEEE Transactions on Electron Devices.* 50(9): 1926-1933.
[8] Sanjeet Kumar Sinha, Saurabh Chaudhury. 2012. Simulation and Analysis of Quantum Capacitance in Single-Gate MOSFET, Double-Gate MOSFET and CNTFET Devices for Nanometer Regime. *IEEE* 978-1-4673-4700-6/12.
[9] V. C. Chan, T. M. Buehler, D. R. McCamey, A. J. Ferguson, D. J. Reilly, C. Yang, T. Hopf, A. S. Dzurak, A. R. Hamilton, D. N. Jamieson, R. G. Clark. 2005. Single-Electron Transistor Coupled to a Silicon Nano-MOSFET. Micro- and

Nanotechnology: Materials, Processes, Packaging, and Systems II. *Proc. of SPIE* Vol. 5650 0277-786X/05. doi: 10.1117/12.583293.

[10] George, W. Hanson. 2008. *Fundamentals of Nanoelectronics.* New York. Pearson International Edition.

[11] Anisur Rahman, Jing Guo, Supriyo Datta, Mark S. Lundstrom. 2003. Theory of Ballistic Nanotransistors. *IEEE transactions on Electron Devices.* 50(9): 1853-1864.

[12] Mark Lundstrom. 2005. *Notes on the Ballistic MOSFET.* Network for Computational Nanotechnology and Purdue University.

[13] Huang, J. Z., Chew, W. C., Tang, M., Jiang, L. 2012. Efficient Simulation and Analysis of Quantum Ballistic Transport in Nanodevices with AWE. *IEEE Transactions on Electron Devices*. 59(2): 468-476.

[14] Vandana Kunari, Manoj Saxena, R. S. Gupta, Mridula Gupta. 2012. Temperature Dependent Drain Current Model for Gate Stack Insulated Shallow Extension Silicon On Nothing (ISESON) MOSFET for Wide Operating Temperature Range. *Microelectronics Reliability*. 52: 974-983. Elsevier. doi: 10.1016/j.microrel.2011.12.021.

[15] M. P. Anantram, M. S. Lundstrom, D. E. Nikonov. 2007. *Modeling of Nanoscale Devices.* University of Waterloo, Purdue University, Intel Corporation.

[16] Ismail Saad, Khairul A. M., Nurmin Bolong, Abu Bakar A. R, Vijay K. Arora. Computational Analysis of Ballistic Saturation Velocity in Low-Dimensional Nano-MOSFET. *IJSSST*. 12(3). ISSN: 1473-8031 (print).

[17] M. De Michielis, D. Esseni, F. Driussi. Trade-off between Electron Velocity and Density of States in Ballistic Nano-MOSFETs. Google.

[18] Raphael Clerc, Gerard Ghibaudo. Analytical Models and Electrical Characterization of Advanced MOSFETs in the Quasi Ballistic Regime. *International Journal of High Speed Electronics and Systems.* World Scientific Publishing Company.